Joint Inversion of Acoustic and Electromagnetic Wave fields

Scherders, Eva M.L.; Verschuur, D. J.; Van Dongen, K. W.A.

DOI
10.1109/IUS54386.2022.9958627

Publication date
2022

Document Version
Final published version

Published in
IUS 2022 - IEEE International Ultrasonics Symposium

Joint Inversion of Acoustic and Electromagnetic Wave fields

Eva M. L. Scherders
Dept. of Imaging Physics
Delft University of Technology
Delft, the Netherlands

D.J. Verschuur
Dept. of Imaging Physics
Delft University of Technology
Delft, the Netherlands
D.J.Verschuur@tudelft.nl

K.W.A. van Dongen
Dept. of Imaging Physics
Delft University of Technology
Delft, the Netherlands
K.W.A.vanDongen@tudelft.nl

***Abstract*—Imaging by inversion of acoustic or electromagnetic wave fields have applications in a wide variety of areas, such as non-destructive testing, biomedical applications, and geophysical exploration. Unfortunately, each modality suffers from its own application-specific limitations, typically being difficulties in distinguishing different materials/tissues from each other in the case of acoustic wave fields and a low spatial resolution in the case of electromagnetic wave fields. To exploit the advantages of both imaging modalities, we present a Born inversion method where we use an additive regularization term based on structural similarity between the acoustic and electromagnetic contrast. To validate our approach, we compare separate with joint inversion results for one particular example. The results for this example clearly show that separate inversion succeeds in reconstructing the acoustic contrast, but fails to properly reconstruct the electromagnetic contrast. Fortunately, with the joint inversion method, both the acoustic and electromagnetic contrast functions are reconstructed successfully.**

***Index Terms*—Joint inversion, multi-parameter inversion, acoustic, electromagnetic**

I. Introduction

Imaging by inversion of acoustic or electromagnetic wave fields have applications in a wide variety of areas, such as non-destructive testing, geophysical exploration, and biomedical applications. [1], [2] Unfortunately, each modality suffers from its own application-specific limitations, typically being difficulties in distinguishing different materials/tissues from each other in the case of acoustic wave fields and a low spatial resolution in the case of electromagnetic wave fields. To improve the resolution of each modality, one could consider regularization methods that for instance suppress the noise in each image separately. [3] However, these regularization methods often fail in situations where the resulting resolution of a modality is limited by the long wave lengths of the probing wave field and not by the noise in the data. Consequently, instead of improving the outcome of each modality separately, we investigate a method where we use both modalities simultaneously to reconstruct the object. In literature, this approach is referred to as multi-physics or joint inversion methods. [4]–[6] These methods can be based on empirical relations between acoustic and electromagnetic medium properties or on structural similarity. In this work, a joint inversion algorithm based on structural similarity is presented. In particular, we present a Born inversion method with additive regularization based on the L2-norm of the differences in the gradients of the acoustic and electromagnetic contrast.

To present our method, we first formulate the integral equation approach we use for the modeling and inversion of the acoustic and electromagnetic wave fields in the section Theory. Next, we present our numerical examples in the section Results, followed by a discussion and conclusion in the section Conclusion.

II. Theory

This section provides a compact overview of the acoustic and electromagnetic theory used. First, the forward problem is presented followed by a short description of the employed joint inversion method.

A. Forward problem: Acoustic wave fields

The acoustic wave-equation for heterogeneous media in the temporal Fourier domain with angular frequency ω equals [7]

$$\nabla^2\hat{p}(\vec{r}) + \frac{\omega^2}{c_{A,0}^2}\hat{p}(\vec{r}) = -\hat{S}_A^{pr}(\vec{r}) - \omega^2\chi_A(\vec{r})\hat{p}(\vec{r}), \quad (1)$$

where $\hat{p}(\vec{r})$ is the pressure field at the location $\vec{r}$, $\hat{S}_A^{pr}(\vec{r})$ is the primary source term and where the acoustic contrast function $\chi_A(\vec{r})$ is given by

$$\chi_A(\vec{r}) = \frac{1}{c_A^2(\vec{r})} - \frac{1}{c_{A,0}^2}, \quad (2)$$

with $c_A(\vec{r})$ the spatially varying speed of sound, and $c_{A,0}$ the speed of sound of the homogeneous embedding. Note that we use the caret symbol, $\hat{}$, to denote quantities defined in the temporal Fourier domain.

Equation (1) can be cast into an integral equation of the second kind. [8], [9] Within this formulation, the pressure field is written as a superposition of the incident field, $\hat{p}^{inc}(\vec{r})$, generated by the primary sources and propagating in the homogeneous embedding and a scattered field, $\hat{p}^{sct}(\vec{r})$, induced by the contrast source term $\omega^2\chi_A(\vec{r})\hat{p}(\vec{r})$, hence

$$\hat{p}(\vec{r}) = \hat{p}^{inc}(\vec{r}) + \hat{p}^{sct}(\vec{r}). \quad (3)$$

Within the presented formulation, the incident field is obtained by the spatial convolution of the primary source with the

2022 IEEE International Ultrasonics Symposium (IUS) | 978-1-6654-6657-8/22/$31.00 ©2022 IEEE | DOI: 10.1109/IUS54386.2022.9958627

impulse response function of the homogeneous background medium, the Green's function $\hat{G}_A(\vec{r}-\vec{r}')$, hence

$$\hat{p}^{inc}(\vec{r}) = \int_{\vec{r}'\in\mathbb{S}} \hat{G}_A(\vec{r}-\vec{r}')\hat{S}_A^{pr}(\vec{r}')dV(\vec{r}'). \quad (4)$$

Similarly, the scattered field can be described by the convolution of the the contrast source term with the Green's function,

$$\hat{p}^{sct}(\vec{r}) = \omega^2 \int_{\vec{r}'\in\mathbb{D}} \hat{G}_A(\vec{r}-\vec{r}')\chi_A(\vec{r}')\hat{p}(\vec{r}')dV(\vec{r}'). \quad (5)$$

In equations (4) and (5), $\mathbb{S}$ represents the spatial domain where the sources and the receivers are placed, and $\mathbb{D}$ the domain of interest. In 2-D, the volume integrals in equations (4) and (5) reduce to surface integrals, for which the Green's functions equals,

$$\hat{G}_A(\vec{r}-\vec{r}') = \frac{-i}{4}H_0^{(2)}(\omega|\vec{r}-\vec{r}'|/c_{A,0}), \quad (6)$$

where $H_0^{(2)}(\omega|\vec{r}-\vec{r}'|/c_{A,0})$ is the Hankel function of the second kind.

B. Forward problem: Electromagnetic wave fields

The wave equation for the electric field in heterogeneous media in the temporal Fourier domain reads

$$\nabla^2\vec{\hat{E}}(\vec{r}) + \frac{\omega^2}{c_{E,0}^2}\vec{\hat{E}}(\vec{r}) = - \vec{\hat{S}}_E^{pr}(\vec{r}) - \omega^2\chi_E(\vec{r})\vec{\hat{E}}(\vec{r}) + \nabla\left(\nabla\cdot\vec{\hat{E}}(\vec{r})\right), \quad (7)$$

where $\vec{\hat{E}}(\vec{r})$ is the electric wave field, $\vec{\hat{S}}_E^{pr}(\vec{r})$ is the primary source term for the electric field, $\chi_E(\vec{r})$ the electromagnetic contrast function given by

$$\chi_E(\vec{r}) = \frac{1}{c_E^2(\vec{r})} - \frac{1}{c_{E,0}^2}, \quad (8)$$

with $c_E(\vec{r})$ the spatially varying speed of light, and $c_{E,0}$ the speed of light within the homogeneous embedding.

Similar as for acoustic waves, the electric wave field can be described by an integral equation of the second kind, [8], [9]

$$\vec{\hat{E}}(\vec{r}) = \vec{\hat{E}}^{inc}(\vec{r}) + \vec{\hat{E}}^{sct}(\vec{r}), \quad (9)$$

where the incident electric field $\vec{\hat{E}}^{inc}(\vec{r})$ and the scattered electric field $\vec{\hat{E}}^{sct}(\vec{r})$ are given by

$$\vec{\hat{E}}^{inc}(\vec{r}) = \int_{\vec{r}'\in\mathbb{S}} \hat{G}_E(\vec{r}-\vec{r}')\vec{\hat{S}}_E^{pr}(\vec{r}')dV(\vec{r}') \quad (10)$$

and

$$\vec{\hat{E}}^{sct}(\vec{r}) = \omega^2 \int_{\vec{r}'\in\mathbb{D}} \hat{G}_E(\vec{r}-\vec{r}')\chi_E(\vec{r}')\vec{\hat{E}}(\vec{r}')dV(\vec{r}'), \quad (11)$$

where $\hat{G_E}(\vec{r}-\vec{r}')$ is the Green's function for the electric field. In this work, we only consider the TM waves for which the corresponding Green's function is given by [10]

$$\hat{G}_E(\vec{r}-\vec{r}') = \frac{-i}{4}H_0^{(2)}(\omega|\vec{r}-\vec{r}'|/c_{E,0}), \quad (12)$$

where $H_0^{(2)}(\omega|\vec{r}-\vec{r}'|/c_{A,0})$ is the Hankel function of the second kind.

C. Inverse problem

The inverse or imaging problem is the problem where the wave field incident in the embedding and the measured wave field recorded by the receivers on the surface $\mathbb{S}$ are known, but where the contrast and the total wave field within the domain $\mathbb{D}$ are unknown. [1] To linearize this non-linear problem, the Born approximation may be employed, which means that the total field inside the integrals is replaced by the incoming wave field. Within this approximation, the scattered acoustic field (5) reduces to

$$\hat{p}^{sct}(\vec{r}) = \omega^2 \int_{\vec{r}'\in\mathbb{D}} \hat{G}_A(\vec{r}-\vec{r}')\chi_A(\vec{r}')\hat{p}^{inc}(\vec{r}')dV(\vec{r}'), \quad (13)$$

and the scattered electric field (11) to

$$\vec{\hat{E}}^{sct}(\vec{r}) = \omega^2 \int_{\vec{r}'\in\mathbb{D}} \hat{G}_E(\vec{r}-\vec{r}')\chi_E(\vec{r}')\vec{\hat{E}}^{inc}(\vec{r}')dV(\vec{r}'). \quad (14)$$

By employing this approximation, we neglect multiple scattering effects and phase shifts caused by the spatial variations in the speed-of-sound/light.

The reconstruct the unknown contrast functions $\chi_A(\vec{r}')$ and $\chi_E(\vec{r}')$, a conjugate gradient scheme is used that minimizes the L2-norm in the error. This error is defined via the mismatch between the measured and the modeled wave field, where the modeled wave field is based on the reconstructed contrast function. Hence, for each of the two modalities the error functional, $Err^{(n)}$, to be minimized equals

$$Err^{(n)} = \frac{||\hat{f}^{meas} - \hat{G} * (\omega^2\hat{f}^{inc}\chi^{(n)})||_{\mathbb{S}}^2}{||\hat{f}^{meas}||_{\mathbb{S}}^2}, \quad (15)$$

with $\chi^{(n)}$ the updated contrast function, $\hat{G}$ the Green's function, $*$ the spatial convolution operator, and $\hat{f}^{inc}$ and $\hat{f}^{meas}$ the incident and measured scattered field, respectively, all for either the acoustic or electromagnetic field at the n-th iteration. The subscript $\mathbb{S}$ denotes the inner product over ω and the receiver locations $\vec{r}^{rec}\in\mathbb{S}$ for each source.

With the aid of the error functional (15), the acoustic and electromagnetic contrast functions are reconstructed separately. However, to enhance one reconstruction with the aid of information on the shape and location of the other, it may be feasible to sharpen an image that is blurred due to the relative long wave lengths with respect to the size of the unknown object. In this work, we use the difference in gradients of the contrasts as an additional constraint, viz.

$$Err_{GD}^{(n)} = ||\nabla\overline{\chi}_A^{(n)} - \nabla\overline{\chi}_E^{(n-1)}||^2, \quad (16)$$

where $\overline{\chi}_A$ and $\overline{\chi}_E$ are the acoustic and electromagnetic contrast functions, normalized by the maximum of the corresponding absolute real values. The difference in iterations of the normalized contrasts in equation (16) is a result of the fact that the acoustic contrast is updated first followed by an update of the electromagnetic contrast.

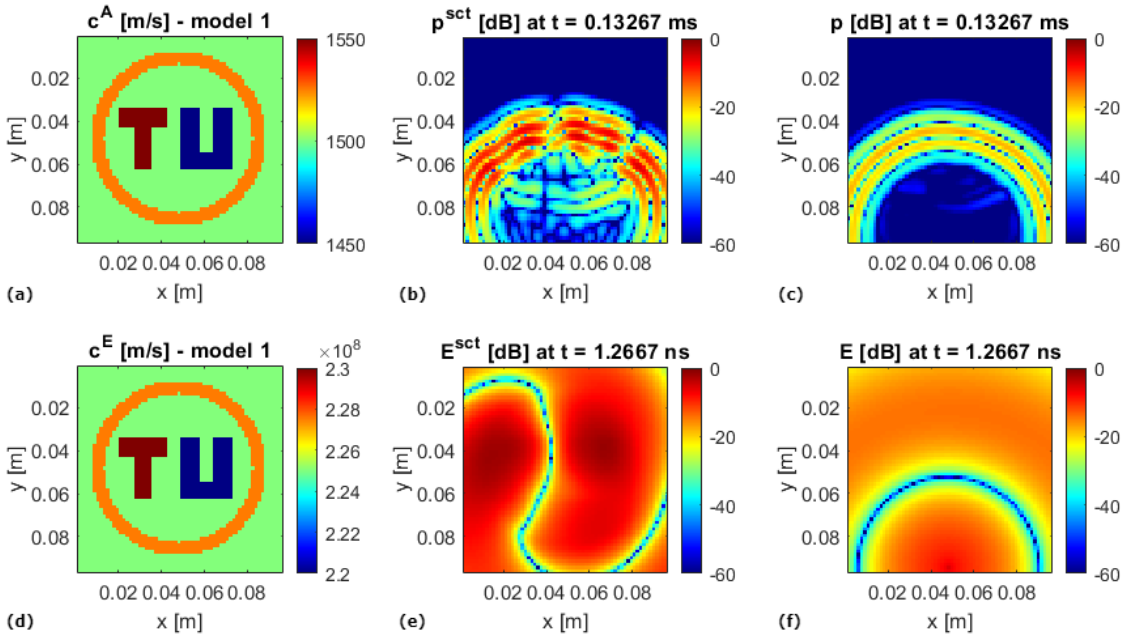

Fig. 1. Forward solution for the acoustic (top) and electromagnetic (bottom) wave fields; synthetic model (a,d) together with snapshots of the scattered (b,e) and total wave field (c,f). Wave fields are on a dB scale.

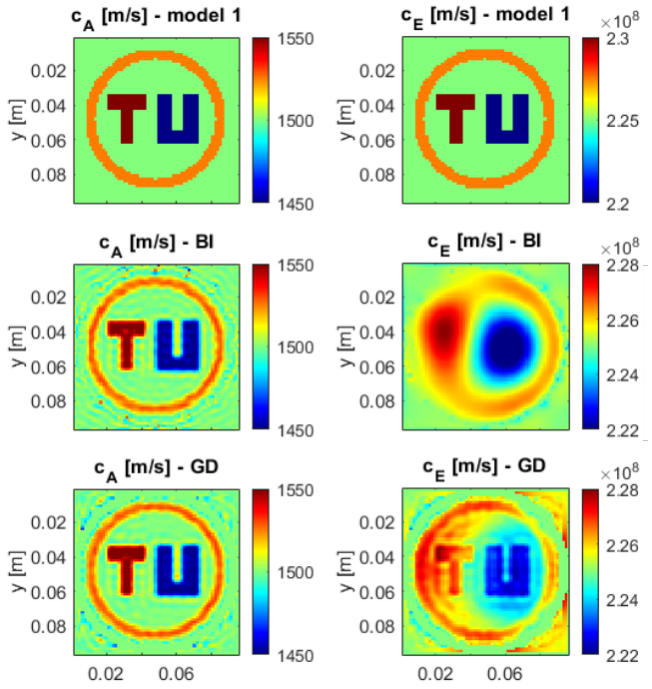

Fig. 2. Inversion results for the acoustic (left) and electromagnetic (right) problem; synthetic model (top), separate inversion (middle), and joint inversion (bottom) using the gradient-difference approach. With separate inversion, only the acoustic contrast function reveals the ring together with the characters "TU" clearly. In order to reconstruct the same profile but, than for the electromagnetic, it is essential to emply joint inversion based on the gradient-difference approach.

III. Results

To test our inversion methods, we emulate a scanner containing 16 sources and 128 receivers all located on a circular ring enclosing the object to be imaged. The object to be imaged is an ring enclosing the characters "TU". The center frequencies of the probing wave fields are 0.1 MHz for the acoustic case and 1 GHz for electromagnetic. Synthetic measurement data is obtained by modeling the acoustic and electromagnetic wave fields using the integral equation method. The employed acoustic and electromagnetic contrast functions alongside with snapshots of the corresponding wave fields are shown in Fig. 1. From these results, it immediately becomes clear that the wave length of the acoustic wave field ($\lambda_{AC} = 15$ mm) is significantly shorter than for the electromagnetic case ($\lambda_{EM} = 225$ mm).

Next, the synthetic measurement data is used is to test our separate and combined inversion methods. The synthetic profiles for the acoustic and electromagnetic contrasts together with the resulting reconstructions after 32 iterations are shown Fig. 2. With separate inversion, the characters "TU" are only clearly visible in the reconstructed acoustic contrast function, but not in the reconstructed electromagnetic contrast. Fortunately, with the aid of the proposed joined inversion method, the characters "TU" also become indisputably visible in the electromagnetic contrast function.

IV. Conclusion

A joint Born inversion algorithm has been developed and tested successfully. With standard Born inversion, an error

functional based on the L2-norm of the mismatch between the measured and modeled wave field is minimized iteratively. To accomplish joint Born inversion, we have extended the standard error functional with an additional penalty term based on the L2-norm of the difference between the normalized gradients of the acoustic and electromagnetic contrasts. The proposed method has successfully been tested on a synthetic model. Speed of sound and light profiles reconstructed by separate and joint Born inversion after 32 iterations have been shown. The mean square errors of the reconstructed profiles are for separate inversion 0.08 for the acoustic and 0.73 for the electromagnetic case, and for joint inversion 0.13 and 0.50, respectively. Therefore, we see that joint inversion leads to a large increase in the resolution of the electromagnetic contrast function as compared to the separate case. For the acoustic reconstruction, joint inversion does not yet show advantages over separate inversion, which is expected given that both contrasts are similar, and, thus, the electromagnetic data does not provide much extra information for the acoustic contrast. Of course, in this particular case, the model fitted the assumption of structural similarity. More experiments are required to investigate situations where the acoustic contrasts and the electromagnetic contrasts are more different.

REFERENCES

[1] N. Ozmen, R. Dapp, M. Zapf, H. Gemmeke, N.V. Ruiter, and K.W.A. van Dongen, "Comparing different ultrasound imaging methods for breast cancer detection," IEEE Transactions on Ultrasonics, Ferroelectrics, and Frequency Control, vol. 62, no. 4, pp. 637–646, 2015.

[2] A.M. Hassan, and M. El-Shenawee, "Review of electromagnetic techniques for breast cancer detection," IEEE Reviews in Biomedical Engineering, vol. 4, pp. 103-118, 2011.

[3] A.B. Ramirez and K.W.A. van Dongen, "Sparsity Constrained Contrast Source Inversion," Journal of Acoustical Society of America, vol. 140, no. 3, pp. 1749-1757, 2016.

[4] O. Ozdemir, A. Oncu and K. W. A. van Dongen, "A Joint Inversion Method for Breast Imaging using Electromagnetic and Acoustics waves," 2018 International Conference on Electromagnetics in Advanced Applications (ICEAA), 2018.

[5] X. Song, M. Li, F. Yang, S. Xu and A. Abubakar, "Three-Dimensional Joint Inversion of EM and Acoustic Data Based on Contrast Source Inversion," IEEE Journal on Multiscale and Multiphysics Computational Techniques, vol. 5, pp. 28-36, 2020.

[6] Y. Zhang, Z. Zhao, Z. Nie and Q. H. Liu, "Approach on Joint Inversion of Electromagnetic and Acoustic Data Based on Structural Constraints," IEEE Transactions on Geoscience and Remote Sensing, vol. 58, no. 11, pp. 7672–7681, 2020.

[7] U. Taskin, N. Ozmen, H. Gemmeke, and K.W.A. van Dongen, "Modeling breast ultrasound; on the applicability of commonly made approximations," Archives of Acoustics, vol. 43, no. 3, pp. 425-435, 2018.

[8] J.T. Fokkema, and P.M. van den Berg, "Seismic applications of acoustic reciprocity," Elsevier, 1993 (ISBN 0-444 89044 0).

[9] A.T. de Hoop, "Handbook of Radiation and Scattering of Waves," London, Academic Press, 1995.

[10] N. Joachimowicz, C. Pichot and J. P. Hugonin, "Inverse scattering: an iterative numerical method for electromagnetic imaging," IEEE Transactions on Antennas and Propagation, vol. 39, no. 12, pp. 1742-1753, 1991.